JOURNAL OF MATERIALS SCIENCE 21 (1986) 3528–3538

Analytical model for the swelling of sintered iron oxide pellets during the haematite–magnetite transformation

M. JALLOULI
Ecole Nationale de l'Industrie Minière, Rabat, Morocco
F. AJERSCH
Ecole Polytechnique, Département de Génie métallurgie, CP 6079, Succursale "A", Montréal, Québec H3C 3A7, Canada

An analytical model for the swelling of sintered iron oxide pellets was developed, based on the variation of the elastic properties arising from the crystallographic and morphological changes that occur during a reduction reaction. The model is restricted to the haematite–magnetite transformation since this phase change was found to represent the largest overall volume increase of the reduction process. It is proposed that this swelling is the result of forces causing sequential fissurization of the bonds between the grains undergoing chemical and structural changes. The relative compressive strengths of the haematite and magnetite particles, the porosity and the pellet morphology are major parameters of the model. Equations of swelling for topochemical and non-topochemical types of reduction are developed independently. The relative contribution of each type of reduction mechanism was found to depend on the effect of the additive agent in the pellet. The model was successfully tested by comparison with experimental swelling results for certain SiO_2, Al_2O_3, CaO and MgO additions.

1. Introduction

The swelling of iron oxide pellets during reduction has been extensively reported in the literature from both theoretical and industrial viewpoints. Most authors agree on the fact that the expansion of the pellets which results during the initial stages of reduction is primarily due to the transformation of hexagonal haematite to cubic magnetite. In order to be able to understand the overall swelling phenomena during reduction, it is essential to consider the volume changes for each transformation. Experiments carried out under controlled-atmosphere conditions have clearly shown that when the contribution to swelling during each phase transformation ($Fe_2O_3 \rightarrow Fe_3O_4 \rightarrow FeO \rightarrow Fe$) was measured [1], the haematite to magnetite transformation represents the largest volume increase (80 to 90% of the maximum swelling value).

The objective of this study is to be able to predict the pellet volume changes from the reducibility results, based on an analysis of the stresses and strains generated during the transformation.

A number of studies have proposed that swelling was due to the distortion of the crystal lattice during reduction. Bleifuss [2], for example, contends that the diffusion of oxygen along the different lattice planes leads to an increase in interplanar distance of 5.7% going from 0.229 nm for $d(0\,0\,0\,1)$ for haematite to 0.242 nm for $d(1\,1\,0)$ for magnetite. He considers that the expansion occurs in the directions of the 1 1 1 plane of magnetite and along the 0 0 0 1 plane of haematite, and that contractions occur in directions parallel to these planes. He concludes that a swelling of 16.5% can be calculated theoretically by this method. Ottow [3], on the other hand, finds that a swelling of only 11% can be calculated from the anisotropic transformation of haematite crystals.

Gorbachev and co-workers [4–8] were among the first to use the elasticity theory to explain the mechanism of fissurization of pellets during reduction. They also used this approach to predict the volume changes of iron-ore sinter during the various heating and cooling cycles and their variation with respect to chemical composition [9–14]. Shigaki *et al.* [15] have also used this model to analyse the structural changes of sinter during reduction.

In this study, the elasticity concept has been used to develop an analytical model to predict the kinetics of swelling of a pellet consisting of sintered haematite particles. Experimentally determined reducibility and swelling curves relating the reducibility–swelling data were then compared with the results predicted by the model. Using this approach an attempt is made to quantify parameters such as chemical composition, porosity, reducing temperature and the nature of the reducing agent, all of which affect swelling characteristics. More specifically, the model is applied only to the haematite–magnetite transformation, which represents the largest volume change.

0022–2461/86 $03.00 + .12

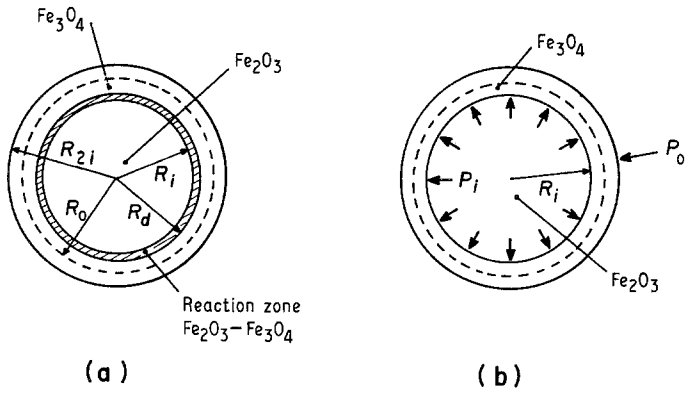

Figure 1 Schematic representation of (a) phase regions of a topochemical reduction by a thin reaction zone and (b) pressure components acting on the transformed layer.

2. Swelling of a solid pellet during topochemical reduction

Consider a solid pellet of haematite of initial radius R_0, undergoing topochemical reduction as shown in Fig. 1a. During the transformation the magnetite–haematite interface moves radially inwards and the pellet expands from R_0 to R_{2i}. The reaction zone occurs in a very finite layer $R_d - R_i$ and the lattice changes from hexagonal haematite to cubic magnetite are assumed to result in stresses applied at the radius R_i, the outermost surface of the non-transformed haematite. In spite of its different crystalline structure, the shell of magnetite of thickness $R_{2i} - R_d$ can be considered to be equivalent to the geometry of a hollow sphere.

A force balance on a hollow sphere with different external and internal pressures is then used to represent the incremental radial displacement of this shell. A number of assumptions are made in order to be able to formulate the analytical treatment:

1. The non-reacted core is much more rigid than the outer shell of magnetite.
2. An effective Young's modulus for porous materials with effective Poisson's ratios is proposed for both haematite and magnetite.
3. The thickness of the diffusion layer (reaction zone) is negligible with respect to the thickness of the transformed outer shell (Fig. 1b).
4. The forces applied on the shell surface can be represented by a uniform pressure P_i at $r = R_i$, and the pressure at $r = R_{2i}$ is considered negligible.

The resulting radial displacement μ_i measured at the surface of the pellet can then be expressed by using Equation A12 of the Appendix to give

$$(\mu_i)_T|_{r=R_i} = \frac{3(1+\nu)}{2E_M}\frac{R_{2i}R_2^3}{R_{2i}^3 - R_i^3}P_i \qquad (1)$$

where ν is Poisson's ratio and E_M is the effective Young's modulus of the porous Fe_3O_4 shell. The subscript T refers to the topochemical nature of the reduction.

This expression is valid only in the elastic range where the equivalent stress remains below the value above which rupture or fissurization can occur. For the case of iron oxide pellets, fissurization often occurs during reduction, and consequently the elastic component becomes very limited. In order to accomodate the fissurization phenomenon, Gorbachev and Shavrin [4] and Alekseyev *et al.* [7] had proposed that, for a specific degree of reduction, the overall expansion can be represented by the sum of n individual displacement steps before fissurization occurs:

$$\mu_n = \sum_{i=1}^{i=n} (\mu_i)_T \qquad (2)$$

where μ_n is the overall displacement for a specific degree of reduction, $(\mu_i)_T$ is the radial displacement of each step before rupture and n is the number of displacement steps.

In order to relate the value of P_i to the position of the reaction interface we can assume that the stresses created during reduction are proportional to the interfacial surface, so that

$$P_i = K_1\frac{R_i^2}{R_0^2} \qquad (3)$$

where K_1 is a proportionally constant directly related to the nucleation and growth of the magnetite phase. This constant depends on the reduction temperature, the gas composition, the surface energy of the haematite grains and finally also on the coherence of the haematite–magnetite interface [16–21].

For the case of a topochemical reduction, the position of the interface can be determined by the overall reduced fraction X_i:

$$X_i = 1 - \left(\frac{R_i}{R_0}\right)^3 \qquad (4)$$

This relation is valid if the thickness of the reaction zone is considered to be negligible. Replacing R_i and P_i by their respective expressions, the equation for the incremental radial displacement of the reaction interface for $X_i > 0$ is given by

$$(\mu_i)_T = K_1\frac{3(1+\nu)}{2E_M}\frac{R_{2i}(1-X_i)^{5/3}}{(R_{2i}/R_0)^3 - (1-X_i)} \qquad (5)$$

The corresponding instantaneous swelling for each step is then

$$(g_i)_T = \frac{[(\mu_i)_T + R_{2i}]^3 - R_{2i}^3}{R_{2i}^3} \qquad (6)$$

and the overall swelling G_n is represented by the summation of all the incremental steps, so that

$$G_n = \sum_{i=1}^{n} (g_i)_T \qquad (7)$$

The overall swelling, however, can also be expressed as a function of the radial displacement of the reaction

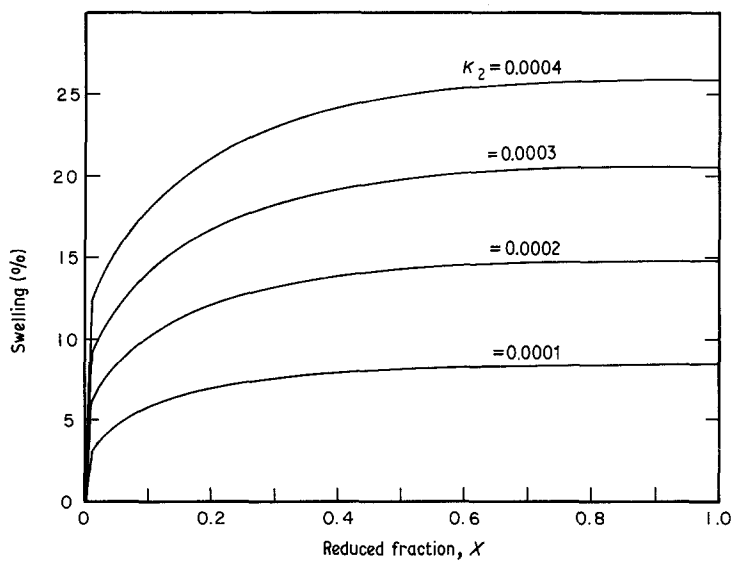

Figure 2 Swelling as a function of the reduced fraction for a topochemical reduction (K_2 variable, n = 100).

front:

$$G_{X_i} = \frac{[(\mu_i)_T + R_{2i}]^3 - R_0^3}{R_0^3} = \frac{V_{X_i} - V_0}{V_0} \quad (8)$$

where V_0 is the initial volume of the pellet and V_{X_i} is the volume corresponding to a reduced fraction X_i. The value of R can then also be respresented by

$$R_{2i} = R_0(1 + G_{X_{i-1}})^{1/3} \quad (9)$$

By substituting into Equation 8 we obtain

$$G_{X_i} = (1 + G_{X_{i-1}})\, K_1 \times \left[\frac{3(1 + \nu)}{2E_M} \frac{(1 - X_i)^{5/3}}{X_i + G_{X_{i-1}}} + 1\right]^3 - 1 \quad (10)$$

For constant temperature and a reducing gas composition, we can therefore write

$$G_{X_i} = (1 + G_{X_i}) \left[K_2 \frac{(1 - X_i)^{5/3}}{X_i + G_{X_{i-1}}} + 1\right]^3 - 1 \quad (11)$$

where

$$K_2 = K_1 \frac{3(1 + \nu)}{2E_M} \quad (12)$$

Equation 12 assumes that the values ν and E_M for the layer of Fe_2O_4 remain constant throughout the reduction.

The swelling curves as a function of the degree of reduction, calculated by Equation 11, are shown in Figs 2 and 3 for different values of n and K_2. These figures show that the curves all decrease monotonically for increasing values of n and K_2. Fig. 4 shows that swelling varies linearly with the product nK_2, and thus these two parameters can be considered to be interdependent.

The number of incremental steps, n, represents the frequency of fissurization of each reduced layer, so that the larger the value of n, the larger will be the fissurization resistance. An increase in K_2 represents an increase in the stresses generated during the haematite–magnetite phase transformation as represented by K_i of Equation 12, or by a decrease in the value of E_M. As a result it can be said that a variation of K_2 directly affects the fissurization frequency, which consequently affects the maximum swelling.

3. Swelling during non-topochemical reduction

For this type of reduction (denoted by the subscript NT) the transformation reaction is assumed to take

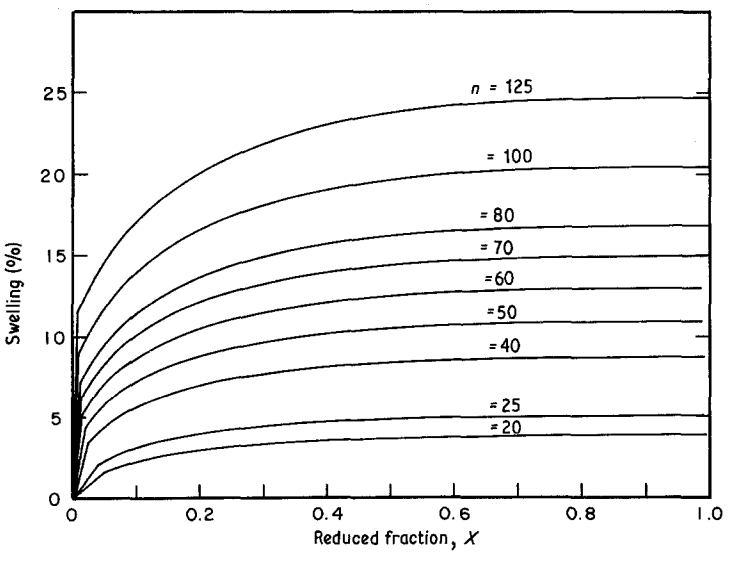

Figure 3 Swelling as a function of the reduced fraction for a topochemical reduction (n variable, K_2 = 0.0003).

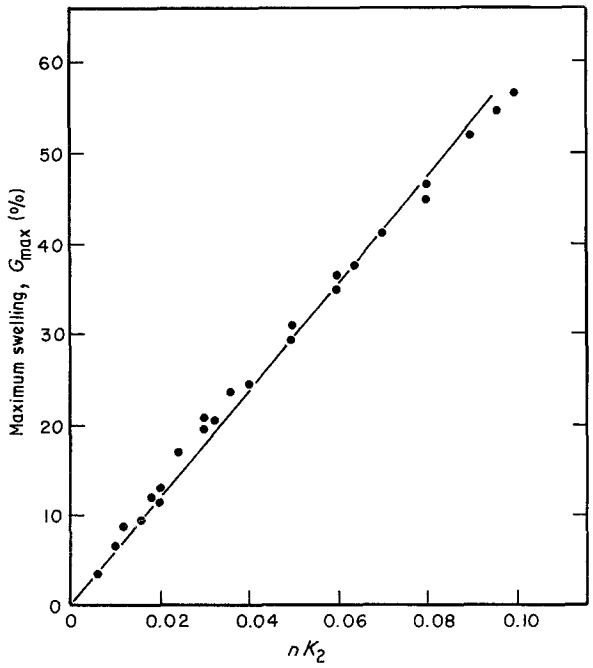

Figure 4 Maximum swelling as a function of nK_2 for topochemical reduction; $G_{max} = 588.23 nK_2$.

place uniformly throughout the pellet. As a first approximation the instantaneous swelling is proportional to the reduced fraction:

$$(g_i)_{NT} \propto (1 - X_i) \tag{13}$$

The instantaneous radial deformation is then represented by the generalized form

$$(\mu_i)_{NT} = K_3 R_{2i}(1 - X_i)^{1/3} \tag{14}$$

where K_3 is a proportionality constant characteristic of the non-topochemical reduction.

If the pellet strength is directly related to an effective Young's modulus E^* we can also write

$$(\mu_i)_{NT} = K_3 R_{2i} \frac{(1 - X_i)^{1/3}}{E^*} \tag{15}$$

where

$$E^* = E_H(1 - X_i) + E_M X_i \tag{16}$$

where E_H is Young's modulus for haematite.

This assumes that the effective overall Young's modulus E^* for the pellet consists of the respective contributions of the values for a haematite and magnetite according to the degree of reduction [4, 22] so that

$$(\mu_i)_{NT} = \frac{K_3}{E_M}\left[\frac{R_{2i}(1 - X_i)^{1/3}}{(E_H/E_M) - X_i[(E_H/E_M) - 1]}\right] = \frac{K_4 R_{2i}(1 - X_i)^{1/3}}{A - X_i(A - 1)} \tag{17}$$

where

$$K_4 = K_3/E_M \tag{18}$$

and

$$A = E_H/E_M \tag{19}$$

The overall swelling can thus be given by a development analogous to the topochemical type reduction, so that

$$G_{X_i} = (1 + G_{X_{i-1}}) \times \left[K_4 \frac{(1 - X_i)^{1/3}}{A - X_i(A - 1)} + 1\right]^3 - 1 \tag{20}$$

Equations 18 and 19 assume that E_M remains constant throughout the reduction and that its value corresponds to the pellet strength when it is completely transferred to magnetite.

Swelling curves determined by Equation 20 for different values of n, A and K_4 are shown in Figs 5 to 7. It is important to note that the swelling rate (dG/dX) depends on the ratio of the respective strengths of haematite and magnetite. Also, when $A = 1$, the the pellet strength remains constant during reduction ($E_M = E_H$) and (dG/dX) is negative and varies very little with respect to X_i.

For large values of A (say $A = 5$), the pellet resistance is greatly decreased during the transformation. This implies that (dG/dX) is positive and is very dependent on the reduced fraction. Experimentally, it is possible to evaluate A by carrying out compression tests at different stages of reduction. Studies have been carried out at reduction temperature for each stage

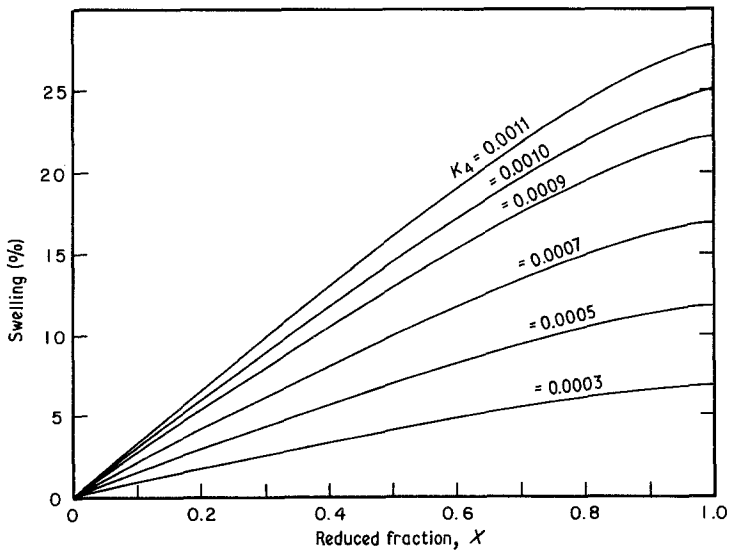

Figure 5 Swelling as a function of reduced fraction for a non-topochemical reduction (K_4 variable, $n = 100$, $A = 1$).

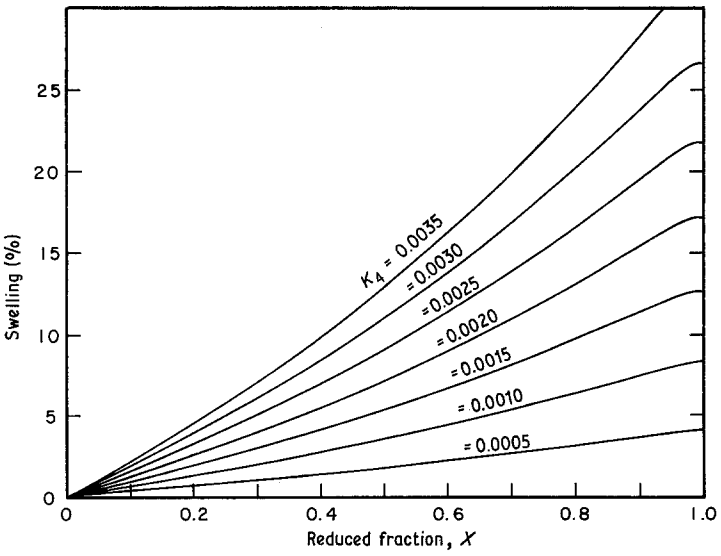

Figure 6 Swelling as a function of reduced fraction for a non-topochemical reduction (K_4 variable, $n = 100$, $A = 5$).

[23, 24] as well as measurements at ambient temperature, of pellets reduced in a Rist type reactor, [25, 26]. The results of Bessières and Becker [27] have also shown that the hardness of a monocrystal of haematite varies in an analogous manner to its variation of compressive strength.

Again, the maximum swelling increases as the value of n increases, as was also observed for the topochemical reduction. The variation of the maximum swelling as a function of A and K_4 is shown in Fig. 8. The parameter E_H/K_3 can be interpreted as the ratio of the initial compressive strength with respect to the stresses generated by the haematite–magnetite transformation. As a result, it becomes clear that the maximum swelling decreases as E_H/K_3 increases, or conversely, the swelling increases as the pellet strength decreases during reduction. Fig. 8 also demonstrates that the pellet must have a high initial compression strength, and must not decrease rapidly as reduction occurs, in order to decrease the swelling characteristics. Experimentally, these two conditions can be controlled by chemical composition and by the pellet induration programme. Normally, initial high compression strength is obtained by high-temperature sintering, whereas the addition of fluxes gives the pellets both hot strength and post-reduction strength.

4. Swelling during reduction controlled by a mixed reaction mechanism

In most cases, pellets are more or less porous and it is probable that the reduction kinetics and subsequent swelling are controlled by a mixed reaction mechanism.

Under these conditions the same assumptions can be applied that were considered in the development of the kinetics of reduction [28, 29]. Assuming that the overall volume change of a reduction with mixed control is the sum of the contributions of all the radial displacement steps from both the topochemical and non-topochemical components,

$$(\mu_i)_{mix} = \alpha(\mu_i)_T + \beta(\mu_i)_{NT} \quad (21)$$

where

$$\alpha + \beta = 1$$

The terms $(\mu_i)_T$ and $(\mu_i)_{NT}$ represent the incremental displacements from the topochemical and non-topochemical contributions, respectively, and the coefficients α and β are parameters which characterize the two kinetic regimes. These parameters are related to the pellet porosity so that their ratio is equivalent to

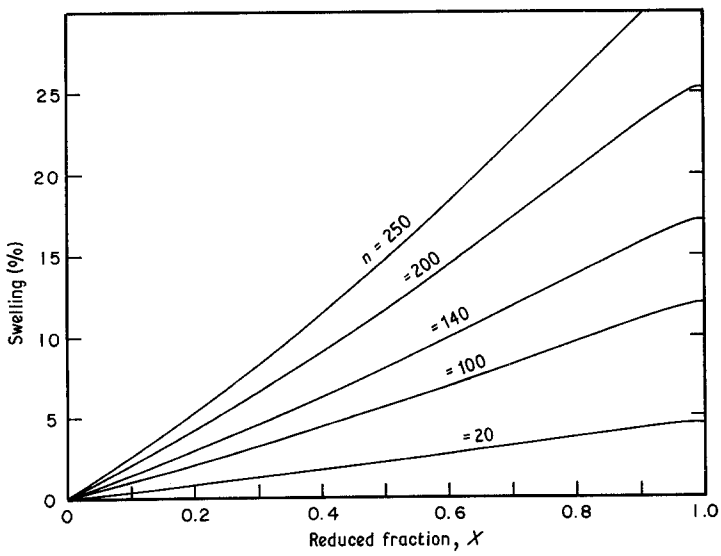

Figure 7 Swelling as a function of reduced fraction for a non-topochemical reduction (n variable, $K_4 = 0.001$, $A = 3$).

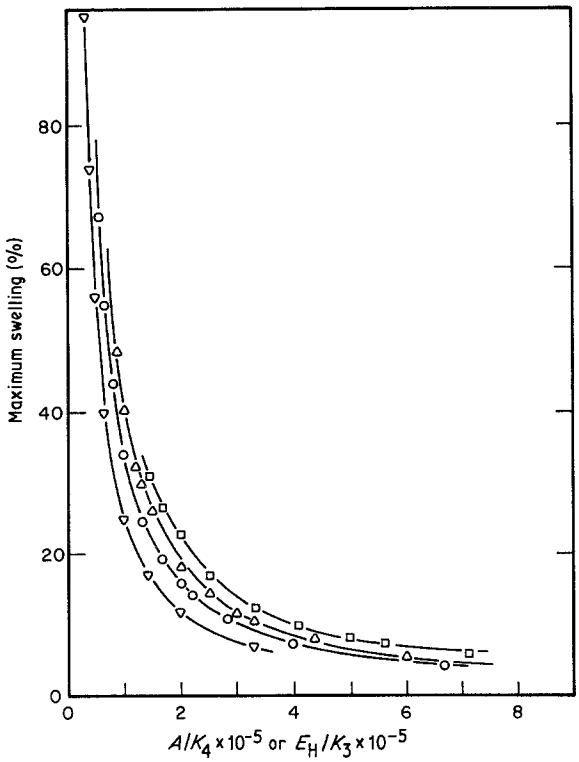

Figure 8 Maximum swelling as a function of parameters A, K_4 and K_3 with $n = 100$ for $A = (\nabla)$ 1, (○) 2, (△) 3 and (□) 5.

the Thiele modulus [30]:

$$\beta/\alpha = K_5 R_0 \frac{D_{\text{eff}}}{k} \tag{22}$$

where K_5 is a parameter which depends on the granulometry and surface characteristics of the pellet, k is the chemical reaction rate constant and D_{eff} is the effective diffusion coefficient within the pores. This coefficient is a function of the Knudsen diffusion and molecular diffusion, as related by

$$\frac{1}{D_{\text{eff}}} = \frac{1}{D_k} + \frac{1}{D_{\text{eff,A,B}}} \tag{23}$$

$$D_{\text{eff,A,B}} = D_{\text{A,B}} \frac{\varepsilon}{\tau} \tag{24}$$

where ε is the pellet porosity, τ is the tortuosity factor and $D_{\text{A,B}}$ is the normal molecular diffusion coefficient of a binary gas (A + B).

It is generally assumed in the literature that $D_{\text{eff,A,B}}$ remains constant during the reduction reaction. On the other hand, it is also necessary that the porosity of the pellet must also increase during reduction when swelling occurs [31, 32]. As a first approximation, we assume that all the swelling is due to an overall change in porosity and that the volume change of the solid-phase components from haematite to magnetite is negligible with respect to the overall swelling, so that

$$\varepsilon_{X_i} = \varepsilon_0 + G_{X_i} \tag{25}$$

where ε_0 is the initial porosity; ε_{X_i} and G_{X_i} are the porosity and swelling at a degree of reduction corresponding to X_i.

Normally, the Knudsen diffusion contribution in Equation 23 is negligible with respect to $D_{\text{eff,A,B}}$ and we can substitute the respective contribution to the displacement equation

$$\begin{aligned}(\mu_i)_{\text{mix}} &= \alpha\left(K_2 \frac{R_{2i}(1 - X_i)^{5/3}}{(R_{2i}/R_0)^3 - (1 - X_i)}\right. \\ &\quad \left. + K_5 R_0 \frac{D_{\text{A,B}} \varepsilon_{X_i}}{k\tau} K_4 \frac{R_{2i}(1 - X_i)^{1/3}}{A - X_i(\text{A} - 1)}\right) \\ &= \alpha\left(K_2 \frac{R_{2i}(1 - X_i)^{5/3}}{(R_{2i}/R_0)^3 - (1 - X_i)}\right. \\ &\quad \left. + K_6 \frac{(\varepsilon_0 + G_{X_i}) R_{2i}(1 - X_i)^{1/3}}{A - X_i(A - 1)}\right)\end{aligned} \tag{26}$$

where

$$K_6 = K_4 K_5 \frac{R_0 D_{\text{A,B}}}{k\tau} \tag{27}$$

Recalling the expression for G_{X_i} in Equation 8, the overall swelling can then be represented in an analogous fashion:

$$\begin{aligned}G_{X_i} &= (1 + G_{X_{i-1}})\left[\alpha\left(\frac{K_2(1 - X_i)^{5/3}}{X_i + G_{X_{i-1}}}\right.\right. \\ &\quad \left.\left. + \frac{K_6(\varepsilon_0 + G_{X_{i-1}})(1 - X_i)^{1/3}}{A - X_i(A - 1)}\right) + 1\right]^3 - 1\end{aligned} \tag{28}$$

In Equation 27 we also neglect the variation of τ as a function of porosity, as well as the variation of the grain size incorporated in the constant K_5. The values of $D_{\text{A,B}}$ and k depend on the temperature and on the composition of the reducing atmosphere, but can be assumed to remain constant for constant reduction rates. The value of K_4, which has the same significance as K_2, and the parameters v and E for the magnetite phase can also be assumed to be constant throughout the transformation to magnetite. Consequently the stresses per unit surface area (K_1) or per unit volume (K_3) generated by the haematite–magnetite transformation are also assumed to remain constant during the reduction.

5. Application of the model to experimental results

The model developed for mixed control was then applied to the swelling of synthetically prepared pellets. Recrystallized haematite, re-crushed to a granulometry of normal iron-ore concentrate, with additions of small amounts of CaO, MgO, Al_2O_3 and SiO_2, was formed into spherical pellets and sintered in a normal induration cycle. These pellets were then reduced in a stage-wise manner using different $CO-CO_2$ atmospheres in order to determine the swelling associated with each phase transformation from Fe_2O_3 to iron [1, 33, 34]. The swelling during reduction was continuously measured using the dilatometric technique previously developed [1]. The reduction kinetics were followed in analogous experiments with identical pellets suspended in a thermobalance.

The calculation of the constants α, K_2 and K_6 from Equation 28 were based on the experimental results of the swelling against reduction data by taking fixed values of n and A. With these constants and the

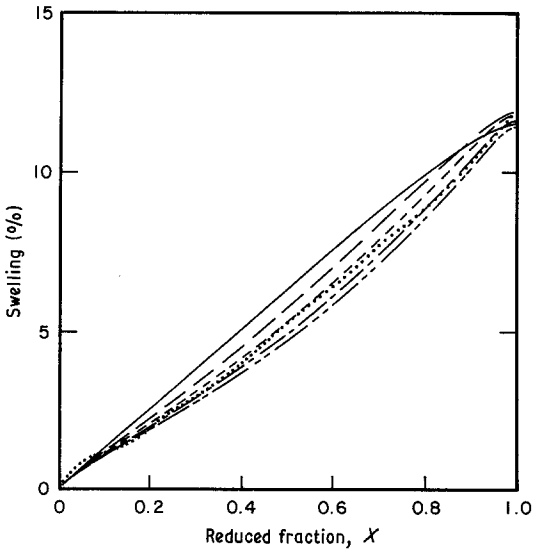

Figure 9 Swelling as a function of reduced fraction calculated from model and compared to experimental results for pellet composition 99.5% Fe_2O_3 + 0.5% CaO, (n = 100); A = (——) 1, (– –) 2, (– – –) 3, (– – –) 4, (– – – –) 5; (· · ·) experimental data.

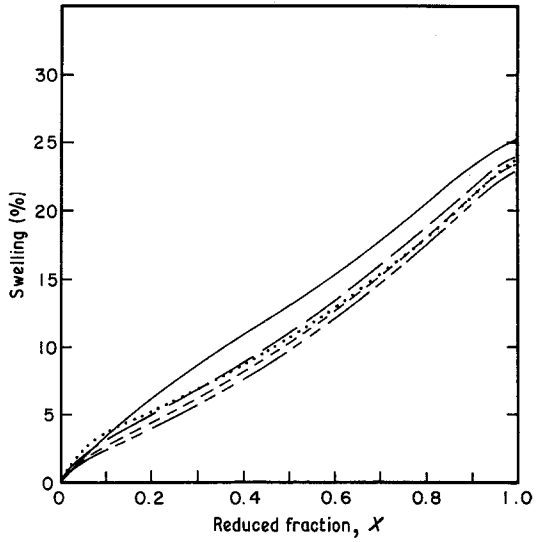

Figure 11 Swelling as a function of reduced fraction calculated from model and compared to experimental results for pellet composition 98.0% Fe_2O_3 + 2.0% Al_2O_3 (A = 3); n = (——) 25, (– –) 50, (– – –) 100, (– – – –) 200; (· · ·) experimental data.

reduction against time curve, one can calculate the corresponding swelling against time curve and compare with the experimental results.

The computer calculation used in this simulation is based on a non-linear regression analysis. The first stage necessitated the determination of the values of n and A to fit to the experimental values of the swelling curve. The value of A can be estimated from the compression strength of the pellets at different reduction levels, and is found to be generally between 2 and 5. On the other hand the parameter n is difficult to determine experimentally. Using the data of Bleifuss [2], Gorbachev and Shavrin [6] have attempted to determine the degree of reduction when fissurization of the grains of haematite occurred. They simply assumed that the elastic properties of haematite and magnetite for a single crystal of volume 1 mm^3 are the same ($E_H = E_M = 2 \times 10^4$) and then calculated that a 5% reduction will result in a critical stress of $\sigma_0 = 10\,kg\,mm^{-2}$ which causes fissurization. This implies that the value of n must be at least 20 in order to describe the swelling phenomena according to the proposed model. The pellet strength, however, does vary as reduction proceeds and according to this analysis will certainly affect the frequency of fissurization. Since the pellets are formed of recrystallized grains of oxide with additions of a binding agent one must also consider the strength of the bonds between these grains.

Figs 9 to 11 show the influence of the variation of A and n on the ability to fit the calculated values to the experimental results. Two different compositions with different swelling maxima are used for comparison. For the case of the pellet containing 0.50% CaO, we can observe that the model best fits the swelling curve for A = 3 and for n = 100. The results also showed that these same values of A and n can represent the

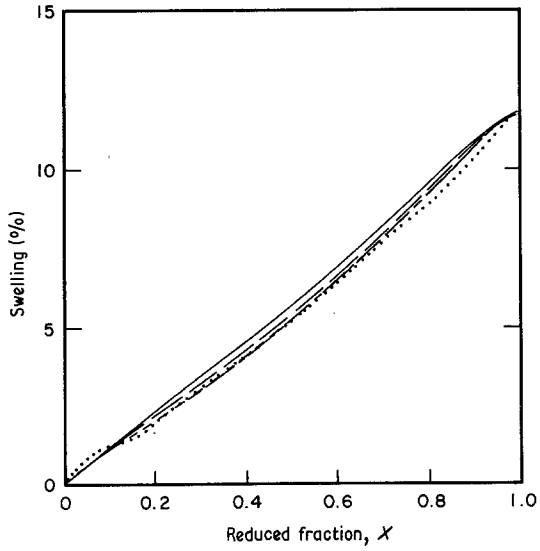

Figure 10 Swelling as a function of reduced fraction calculated from model compared to experimental results for pellet composition 99.5% Fe_2O_3 + 0.5% CaO (A = 3); n = (——) 25, (– –) 50, (– – –) 100, (– – –) 200; (· · ·) experimental data.

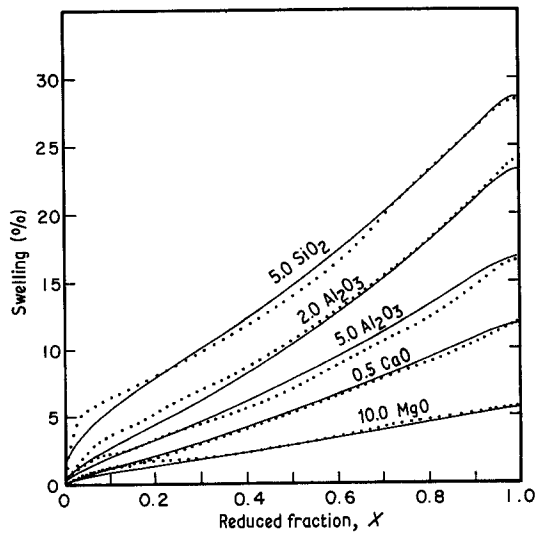

Figure 12 Comparison of (——) model for swelling against reduced fraction with (· · ·) experimental results for pellets of variable composition using n = 100 and A = 3; T = 1223 K.

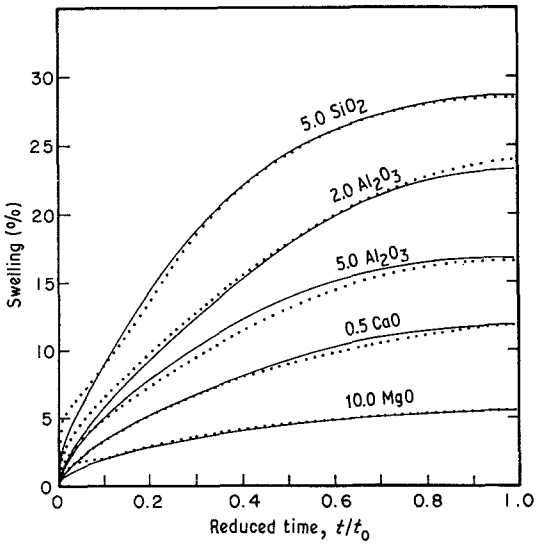

Figure 13 Comparison of (——) model for swelling against relative reduction time with (· · ·) experimental results for pellets of variable composition using $n = 100$ and $A = 3$; $T = 1223$ K.

experimental swelling curves for pellets with a 2% Al_2O_3 addition equally well (Fig. 11).

The variation of the values of α, K_2 and K_6 as a function of A and n are summarized in Table I. The calculated and experimental swelling values are given for complete reduction of all haematite to magnetite ($G_{X=1}$). It should be noted that A and n are interdependent and are functions of the chemical composition of the pellets as well as the reducing conditions. It is thus necessary to be able to evaluate A and n for each type of pellet in order to get the most precise values of α, K_2 and K_6 to best describe the swelling curves.

Values of $n = 100$ and $A = 3$ were used for different composition as shown in Table II. Figs 12 and 13 show that the model is able to predict the swelling kinetics of the pellets for cases when the maximum swelling does not exceed 30%. When swelling rises above this value, major cracks of a different form are generally the cause of swelling which cannot be described by the model, as was observed with pellets containing additions of SiO_2 and MgO. The effect of the different additives on the intergranular strength is difficult to quantify.

The series of results for the samples of different compositions and reduced under different conditions was used to evaluate the topochemical (represented by K_2) and the non-topochemical (respresented by K_6) contributions to the swelling. This analysis is then applied to the swelling curves as a function of reduction (Fig. 14). It can be observed that for all cases, the K_6/K_2 ratio as a function of $(dG/dX)_{x=0}$ is a simple decreasing value. This implies that the initial swelling rate decreases logarithmically as a function of the ratio of the non-topochemical to topochemical contributions. This observation can also be seen in Figs 2 and 3 for the topochemical reduction, and in Figs 5, 6 and 7 for the non-topochemical reduction.

Recently, Hayes and Grieveson [35] investigated the effect of temperature and chemical potential on the morphology of the magnetite produced from solid crystals of haematite. They found that the rate of the haematite–magnetite transformation is controlled by the rate of formation of magnetite nuclei. A low rate leads to higher swelling values according to the relation $G_{max} = K(1/N_R)$ where K is a constant including chemical potential, surface energy change and activation energy, and N_R is the number of magnetite nuclei formed. Conversely, a large number of nuclei therefore results in lower swelling values.

In this study the degree of swelling was related to the internal structure in terms of the β/α ratio. When β/α approaches zero (large values of α) the reaction is mainly topochemical, producing higher values of swelling, whereas when β/α is large, the non-topochemical contribution is predominant, resulting in lower swelling. The topochemical reduction mode allows fewer Fe_3O_4 nuclei to form, since the reaction surface is restricted to a spherical shell as compared to

TABLE I

A	n	98 Fe_2O_3–2Al_2O_3 (porosity = 0.2642, $G_{X=1}$(exp.) = 23.94%)				99.5 Fe_2O_3–0.5 CaO (porosity = 0.2312, $G_{X=1}$(exp.) = 11.995%)			
		$\alpha \times 10^2$	$K_2 \times 10^4$	$K_6 \times 10^2$	$G_{X=1}$(model)(%)	$\alpha \times 10^2$	$K_2 \times 10^4$	$K_6 \times 10^2$	$G_{X=1}$(model)(%)
3	25	8.907	68.060	17.260	24.61	10.550	13.580	11.660	11.56
	50	9.016	7.101	9.832	23.72	7.865	1.871	8.290	11.74
	100	6.708	2.907	6.757	23.94	5.354	0.8842	6.157	11.80
	150	3.379	2.847	9.037	23.30	4.194	0.5707	5.274	11.81
	200	2.675	2.169	8.621	22.81	3.491	0.4201	4.771	11.80
1	100	4.755	2.999	5.045	23.71	2.703	0.6504	6.254	11.53
2	100	5.949	2.985	6.007	23.83	4.320	0.8629	5.951	11.80
4	100	7.321	2.815	7.340	22.69	1.666	3.231	23.660	11.62
5	100	7.923	2.736	7.844	22.10	2.066	2.831	21.890	11.42

TABLE II

Sample composition	Porosity	$\alpha \times 10^2$	$K_2 \times 10^4$	$K_6 \times 10^2$	$G_{X=1}$(exp.)(%)	$G_{X=1}$(model)(%)
95 Fe_2O_3–5SiO_2	0.2647	5.612	12.430	7.419	28.23	28.68
98 Fe_2O_3–2Al_2O_3	0.2642	6.708	2.907	6.757	23.94	23.94
95 Fe_2O_3–5Al_2O_3	0.276	4.832	2.601	7.324	16.48	16.74
99.5 Fe_2O_3–0.5 CaO	0.2312	5.354	0.8842	6.157	11.95	11.80
90 Fe_2O_3–10 MgO	0.3012	3.427	1.855	3.701	5.64	5.56

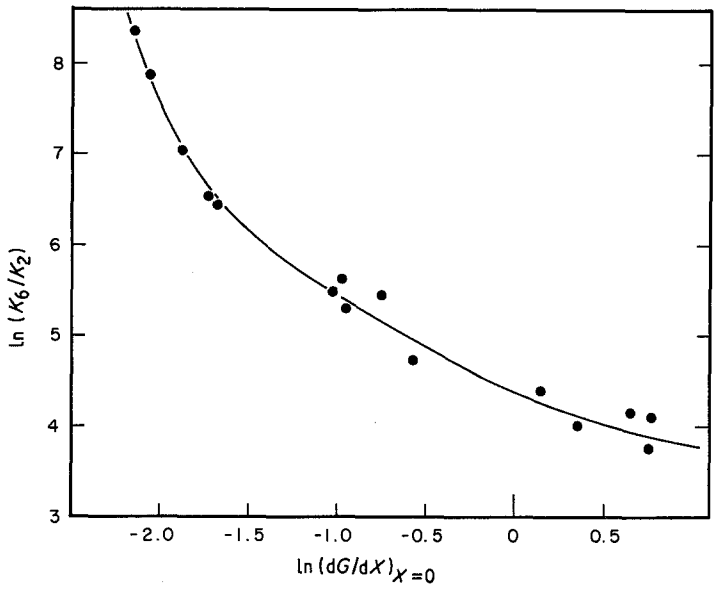

Figure 14 Initial swelling rate as a function of the ratio of the non-topochemical to topochemical contributions for $n = 100$, $A = 3$.

the non-topochemical mode where the nuclei can form on all the particle surfaces within the pellet volume.

The effects of reaction gas composition on the total swelling were previously shown in a series of experiments using pure hydrogen gas and 40% CO–60% N_2 gas mixtures for the reduction of haematite pellets with sodium and potassium additions [36]. Using pure hydrogen, the reduction proceeds at a rate 3 to 5 time faster than with the 40% CO–60% N_2 mixtures, initial rates being even more rapid. Again, this indicates that the high nucleation rate generated with pure hydrogen results in a lower swelling than reduction with 40% CO–60% N_2. Fig. 14 shows that a direct correlation exists between the initial rates of swelling and the ratio of non-topochemical to topochemical contributions. The value of β/α is larger for hydrogen reduction mainly because of the higher value of the effective diffusivity of the H_2–H_2O gas mixture.

The addition of certain other elements, even in small quantities, also changes the morphology during the normal pellet induration cycle and can alter the grain structure due to the formation of a liquid phase. The surface area of the grain as well as the total reaction surface within the pellet is reduced, and thus fewer magnetite nuclei are generated. This again leads to a more topochemical type of reaction with larger swelling values, with fewer but larger fissures, as compared to the non-topochemical case.

The limits of application of this model are directly related to the ability of the pellet to retain its spherical shape during the microfissurization process which is the basis of swelling. This implies that the swelling should be in the normal rather than in the catastophic range (less than 30% volume increase) and that the pellet undergoes only solid–solid phase transformations. It cannot accomodate large fissures which cause an uneven distribution of the forces acting on the non-reduced phase. In certain cases small amounts of sodium, potassium and calcium oxides can react to form a liquid phase during the reduction period and thus change the morphology even more drastically. In this case the pellets undergo plastic rather than elastic deformation. This type of catastrophic swelling cannot be quantified by the model, but does predict higher values since the ratio $E_H/E_M = A$ becomes very large because of the greatly reduced value of the compressive strength (E_M) of the reduced phase.

Experiments still need to be carried out in order to evaluate the compressive strengths E_H and E_M for each type of pellet, as well as for the determination of other constants in order to be able to use the model in other specific cases.

6. Conclusion

An analytic model based on the theory of elasticity was applied to the kinetics of reduction of spherical iron oxide pellets with small additions of CaO, MgO, Al_2O_3 and SiO_2 during the haematite–magnetite transformation. The stresses resulting from the crystallographic change were related to the overall deformation of the pellet resulting in normal swelling of the pellet.

The model has also shown that the contributions to the swelling behaviour are influenced by parameters such as the reducing conditions, the oxygen potential, the chemical composition of the reducing gas and the morphology of the pellet.

Appendix: Static equilibrium equations for an isotropic hollow sphere

Consider a hollow sphere of external radius R_2 with a uniform pressure P_2 applied at its external surface, and a uniform pressure P_1 applied at a radius R_1. The analytic solution for this configuration is given in detail by Landau and Lifshitz [37].

Neglecting gravitational effects and assuming isotropic properties, the general force balance can be written as

$$2(1 - v)\bar{\nabla}(\bar{\nabla} \cdot \bar{\mu}) = 0 \qquad \text{(A1)}$$

where v is the Poisson coefficient; here

$$\bar{\nabla} = \left(\frac{\delta}{\delta_x}\bar{i} + \frac{\delta}{\delta_y}\bar{j} + \frac{\delta}{\delta_z}\bar{h}\right)$$

and μ is the displacement vector ($\bar{\mu} = \bar{\mu}_{xi} + \bar{\mu}_{yj} + \bar{\mu}_{zh}$).

Integration of Equation A1 gives

$$\bar{\nabla} \cdot \bar{\mu} = a \tag{A2}$$

where a is a constant.

In spherical coordinates, the divergence of the vector μ can be written as

$$\nabla \cdot \mu = \frac{1}{r^2} \frac{d(r^2 \mu)}{dr} = a \tag{A3}$$

Integrating,

$$\mu = \frac{a}{3} r + \frac{b}{r^2} \tag{A4}$$

where b is also a constant. The radial strain ε_r is given by

$$\varepsilon_r = \frac{\mu_r}{r} = \frac{a}{3} - \frac{2b}{r^3} \tag{A5}$$

and, for an isotropic material, the tangential components ε_θ and ε_ϕ are equal so that

$$\varepsilon_\theta = \varepsilon_\phi = \frac{\mu_r}{r} = \frac{a}{3} + \frac{b}{r^3} \tag{A6}$$

The radial and tangential stresses are then found by using Hooke's law:

$$\sigma_r = \frac{E}{(1 + \nu)(1 - 2\nu)} [(1 - \nu)\varepsilon_r + 2\nu\varepsilon_\phi]$$

$$= \frac{E}{(1 - 2\nu)} \frac{a}{3} - \frac{2E}{(1 + \nu)} \frac{b}{r^3} \tag{A7}$$

and

$$\sigma_\phi = \frac{E}{(1 + \nu)(1 - 2\nu)} [(1 - \nu)\varepsilon_\phi + \nu(\varepsilon_\phi + \varepsilon_r)]$$

$$= \frac{E}{(1 - 2\nu)} \frac{a}{3} + \frac{E}{(1 + \nu)} \frac{b}{r^3} \tag{A8}$$

where E is Young's modulus. The constants a and b can be found by using the boundary conditions:

$$r = R_1, \quad \sigma_r = -P_1$$

$$r = R_2, \quad \sigma_r = -P_2$$

so that

$$a = \frac{3P_1R_1^3 - 3P_2R_2^3}{R_2^3 - R_1^3} \frac{(1 - 2\nu)}{E} \tag{A9}$$

and

$$b = \frac{R_1^3 R_2^3 (P_1 - P_2)}{R_2^3 - R_1^3} \frac{(1 + \nu)}{2E} \tag{A10}$$

Substituting into Equation A4, the radial displacement becomes

$$\mu_r = \frac{(1 - 2\nu)}{E} \left(\frac{P_1R_1^3 - P_2R_2^3}{R_1^3 + R_2^3} \right) r + \frac{(1 + \nu)}{2E} \left(\frac{R_1^3 R_2^3 (P_1 - P_2)}{R_2^3 - R_1^3} \right) \frac{1}{r^2} \tag{A11}$$

so that at the surface of the sphere, when $r = R_2$ and $P_2 = 0$,

$$\mu_r \Big|_{\substack{r = R_2 \\ P_2 = 0}} = \frac{3(1 + \nu)}{2E} \frac{R_2 R_1^3}{R_2^3 - R_1^3} P_1 \tag{A12}$$

Acknowledgements

The authors would like to express their appreciation to Y. Blanchette for the computer simulation of the swelling curves, to J. Lanteigne of IREQ for his helpful discussions in developing the model, as well as to the Natural Sciences and Engineering Research Council and SIDBEC–NORMINES for their financial support.

References

1. M. JALLOULI, PhD thesis, Ecole Polytechnique, Montreal (1981).
2. R. L. BLEIFUSS, in Proceedings of International Conference on Science and Technology of Iron and Steel, Suppl. II, *Trans. Iron Steel Inst. Jpn* (Tokyo, 1971) p. 52.
3. M. OTTOW, PhD thesis, Technische Hochschule, Berlin (1966).
4. V. A. GORBACHEV and S. G. SHAVRIN, *Steel USSR* **9** (10) (1979) 495.
5. *Idem, Russ. Metall.* (3) (1980) 18.
6. *Idem, ibid.* (2) (1980) 16.
7. L. F. ALEKSEYEV, V. A. GORBACHEV and S. V. SHAVRIN, *ibid.* (5) (1980) 9.
8. *Idem, ibid.* (6) (1980) 16.
9. N. P. ALEKSEEVA, V. V. KASHIN, V. B. FETISOV and B. Z. KUDINOV, *Steel USSR* **8**(9) (1978) 187.
10. A. P. BUTKAREV, V. A. GORBACHEV, G. M. MAYZEL' and S. V. SHAVRIN, *Russ. Metall.* (2) (1979) 42.
11. A. P. BUTKAREV, V. A. GORBACHEV, G. M. MAYZEL', A. V. CHENTZOV and S. V. SHAVRIN, *ibid.* (6)
12. *Idem, Steel USSR* **9**(2) (1979) 57.
13. L. F. ALEKSEEV, V. A. GORBACHEV, G. M. MAYZEL', T. V. SAPOZHNIKOVA and S. V. SHAVRIN, *ibid.* **9** (6) (1979) 265.
14. V. M. ABZALOV, V. A. GORBACHEV, G. M. MAYZEL', A. V. CHENTZOV and S. V. SHAVRIN, *ibid.* **9**(6) 1979) 26.
15. I. SHIGAKI, M. SAWADA, M. MAEKAWA and K. NARITA, *Trans. Iron Steel Inst. Jpn.* **22** (1982) 839.
16. J. O. EDSTROM, *J. Iron Steel Inst.* **175** (1953) 289.
17. H. BRILL-EDWARDS, B. L. DANIELL and R. L. SAMUEL, *ibid.* **203** (1965) 361.
18. A. V. BRADSHAW and A. G. MATYAS, *Met. Trans. B* **7B** (1976) 81.
19. J. R. PORTER and P. R. SWANN, *Ironmaking & Steelmaking* **4**(5) (1977) 300.
20. P. R. SWANN and N. J. TIGHE, *Met. Trans. B* **8B** (1977) 479.
21. P. C. HAYES and P. GRIEVESON, *ibid.* **12B** (1981) 579.
22. J. LANTEIGNE, R. ROBERGE, H. LEHUY, J. L. FIHEY and S. FONER, *IEEE Trans. (Magn.)* **17** (1) (1981) 265.
23. H. BRILL-EDWARDS, H. E. N. STONE and B. L. DANIELL, *J. Iron Steel Inst.* **207** (1969) 1565.
24. M. D. PEPPER and B. L. DANIELL, *ibid.* **208** (1970) 553.
25. C. OFFROY, *Rev. Métall.* **66** (1969) 491.
26. Y. RIQUIER and M. NOURRICIER, *Métallurgie* **XI** (4) (1971) 204.
27. A. BESSIERES and P. BECKER, *Métall. Mem. Etudes Sci. Rev.* **77** (1980) 1021.
28. J. SZEKELEY, J. W. EVANS and H. Y. SOHN, "Gas Solid Reactions" (Academic Press, New York, 1976) p. 125.
29. H. Y. SOHN and M. E. WADSWORTH, "Rate Processes of Extractive Metallurgy" (Plenum Press, New York, 1979) p. 30.
30. E. W. THIELE, *Ind. Eng. Chem.* **31** (1939) 916.
31. S. TANIGUCHI, M. OHMI and H. FUKUHARA, *Trans. Iron Steel Inst. Jpn.* **18** (1978) 633.
32. S. TANIGUCHI and M. OHMI, *Trans. Jpn. Inst. Met.* **19** (1978) 581.
33. M. JALLOULI, M. RIGAUD and F. AJERSCH, in Proceedings of 3rd International Symposium on Agglomeration, Nurnberg, 1981, edited by O. Molerus and W. Hufnagel (Nurnberger Messe und Ausstellungsgesellschaft, Messencentrum) p. B81.
34. M. JALLOULI, F. AJERSCH and M. RIGAUD, in

Proceedings of International Symposium on the Physical Chemistry of Iron and Steelmaking, Toronto, August 1982 (Metallurgical Society of CIM) p. IV-11.
35. P. C. HAYES and P. GRIEVESON, *Met. Trans.* **12B** (1981) 319.
36. F. AJERSCH, PEI HE-NIAN and M. JALLOULI, in Proceedings of the 4th Symposium on Agglomeration (Publication AIME-155, AIME, Warrendale, Pennsylvania, 1985) p. 259.
37. L. D. LANDAU and E. M. LIFSHITZ, "Theory of Elasticity", 2nd Edn (Pergamon, New York, 1975).

Received 2 July 1984
and accepted 18 December 1985